How to cite: *Angew. Chem. Int. Ed.* **2024**, *63*, e202401541
doi.org/10.1002/anie.202401541

Immunochemistry Hot Paper

Deciphering the Chemical Language of the Immunomodulatory Properties of *Veillonella parvula* Lipopolysaccharide

Molly Dorothy Pither[+], Emanuela Andretta[+], Giuseppe Rocca, Fabio Balzarini, Alejandra Matamoros-Recio, Roberta Colicchio, Paola Salvatore, Yvette van Kooyk, Alba Silipo, Francesca Granucci, Sonsoles Martin-Santamaria, Fabrizio Chiodo, Antonio Molinaro, and Flaviana Di Lorenzo**

Abstract: *Veillonella parvula*, prototypical member of the oral and gut microbiota, is at times commensal yet also potentially pathogenic. The definition of the molecular basis tailoring this contrasting behavior is key for broadening our understanding of the microbiota-driven pathogenic and/or tolerogenic mechanisms that take place within our body. In this study, we focused on the chemistry of the main constituent of the outer membrane of *V. parvula*, the lipopolysaccharide (LPS). LPS molecules indeed elicit pro-inflammatory and immunomodulatory responses depending on their chemical structures. Herein we report the structural elucidation of the LPS from two strains of *V. parvula* and show important and unprecedented differences in both the lipid and carbohydrate moieties, including the identification of a novel galactofuranose and mannitol-containing O-antigen repeating unit for one of the two strains. Furthermore, by harnessing computational studies, in vitro human cell models, as well as lectin binding solid-phase assays, we discovered that the two chemically diverse LPS immunologically behave differently and have attempted to identify the molecular determinant(s) governing this phenomenon. Whereas pro-inflammatory potential has been evidenced for the lipid A moiety, by contrast a plausible "immune modulating" action has been proposed for the peculiar O-antigen portion.

Introduction

Veillonella genus is a key member of the healthy human microbiota, found to colonize the oral cavity, gastrointestinal tract, throat, and vagina.[1–5] However, growing evidence suggests that *Veillonella* genus may also act as an opportunistic pathogen or as an "accessory pathogen", by promoting the growth of pathogenic species particularly within oral biofilms.[1,6] Divergent abilities of various *Veillonella* strains to behave as commensals or as pathogens remain concealed at the strain level.

Herein we focus on *V. parvula*, an essential member of the healthy oral microbiota that is also commonly found enriched in the intestine of patients affected by inflammatory bowel disease,[7,8] alcohol-associated liver disease,[9] or Hirschsprung's disease.[10] The positive correlation between inflammation and *V. parvula* abundance in the human intestine has suggested the capability of this versatile bacterium to harness conditions present during inflammation to colonize the intestine.[11] However, as a potential pathobiont, the role of *V. parvula* in the development of inflammatory-related diseases remains to be investigated. In

[*] Dr. M. D. Pither,[+] Dr. E. Andretta,[+] Prof. A. Silipo, Prof. A. Molinaro, Prof. F. Di Lorenzo
Department of Chemical Sciences
University of Naples Federico II
via Cinthia, 4, 80126, Naples, Italy
E-mail: molinaro@unina.it
flaviana.dilorenzo@unina.it

Mr. G. Rocca, Prof. F. Granucci
Department of Biotechnology and Biosciences
University of Milano-Bicocca
Piazza dell'Ateneo Nuovo, 1, 20126, Milan, Italy

Mr. F. Balzarini, Prof. Y. van Kooyk, Dr. F. Chiodo
Department of Molecular Cell Biology and Immunology
Amsterdam UMC, Vrije Universiteit Amsterdam
1007 MB Amsterdam, The Netherlands

Dr. A. Matamoros-Recio, Prof. S. Martin-Santamaria
Department of Structural and Chemical Biology
Centro de Investigaciones Biológicas, CIB-CSIC
C/ Ramiro de Maeztu, 9, 28040, Madrid, Spain

Dr. R. Colicchio, Prof. P. Salvatore
Department of Molecular Medicine and Medical Biotechnology
University of Naples Federico II
Via Pansini, 5, 80131, Naples, Italy

Dr. F. Chiodo
Institute of Biomolecular Chemistry
National Research Council (CNR)
Via Campi Flegrei, 34, 80078, Pozzuoli, Naples, Italy

[+] Equal contribution.

this scenario, we concentrated on the main constituent of its outer membrane, the lipopolysaccharide (LPS). LPS (or smooth-type LPS, S-LPS) is a complex glycoconjugate consisting in a glycolipid portion termed lipid A, a core oligosaccharide (core OS), and a polysaccharide region (O-antigen).[12] When the O-antigen is absent, the terminology employed is lipooligosaccharide (or rough-type LPS, R-LPS).[12] LPS is known as a potent stimulator of the host immune response, and it has been extensively studied for its negative impact on the development and exacerbation of diseases caused by Gram-negative infections. [12] Nevertheless, recent studies have uncovered LPSs from specific gut commensals playing an active role in maintaining immune homeostasis via immunomodulatory signaling. [12,13] The differential immunopotential of LPSs is correlated to their structure; therefore, on the basis of key chemical features, an LPS can potently, weakly, or not trigger the immune response, which typically culminates in the production of pro-inflammatory mediators. In this frame, deciphering the molecular details of the interaction(s) occurring between LPS and its receptors, and the subsequent signaling pathways that lead to disease *vs* tolerance is of unquestionable importance.

To this aim, we have analyzed the LPS isolated from two strains of *V. parvula*: the strain DSM 2008 and the strain 118(3), isolated from the human intestinal and oral tract, respectively. The structure of the LPS from both strains was determined by the combined use of chemical, spectroscopic and spectrometric techniques, which unveiled important structural differences in both the carbohydrate and lipid moieties. Furthermore, we have evaluated the impact of both LPSs on the innate immune system by using both in vitro human cell models and computational studies and have inspected LPS binding activity to specific lectins known to shape immune responses. We discovered that the two chemically distinct LPSs immunologically behave differently and have attempted to identify the molecular determinant(s) responsible for this behavior.

Results and Discussion

Structural elucidation of LPS from V. parvula

LPS was obtained from dried bacterial cells as reported[14–16] (see Supporting Note 1 in the Supporting Information). The nature and degree of purity was analyzed by SDS-PAGE followed by silver nitrate staining, which disclosed that *V. parvula* DSM 2008 (hereafter referred to as DSM 2008) synthesizes a smooth-type LPS (S-LPS), while *V. parvula* 118(3) (hereafter referred to as 118(3)) produces a R-LPS (Figure S1). Monosaccharide analysis of 118(3) R-LPS revealed the occurrence of terminal D-glucopyranose (Glc*p*), terminal D-galactopyranose (Gal*p*), 6-substituted amino-D-glucopyranose (Glc*p*N), 3,4-disubstituted L,D-heptopyranose (Hep*p*), 2,4-disubstituted L,D-Hep*p*, terminal and 4,5-disubstituted 3-deoxy-D-*manno*-oct-2-ulopyranusonic acid (Kdo*p*). By contrast, DSM 2008 S-LPS displayed the presence of 3-substituted D-Gal*p*, terminal D-Glc*p*N, and 6-substituted D-galactofuranose (Gal*f*). In addition, monosaccharide analysis upon dephosphorylation and reduction revealed the presence for the sole DSM 2008 S-LPS of mannitol, which was found to be not deuterated and consequently did not originate from any mannose present. The investigation of the fatty acid content revealed a distinctive pattern that consisted in the presence of branched acyl chains in the R-LPS of the strain 118(3) which were not detected for the S-LPS of DSM 2008 (Table S1). The stereochemistry of *anteiso*-branched acyl moieties remains to be defined.

The convergent information from chemical analyses, matrix-assisted laser desorption/ionization-time of flight MS (MALDI-TOF MS) and tandem MS (MS/MS), as well as NMR spectroscopy allowed the determination of the full structure of both types of LPS. Indeed, to obtain structural information on the carbohydrate and lipid portions, a mild acid hydrolysis was executed on an aliquot of each sample to selectively cleave the linkage between the Kdo and the non-reducing GlcN of the lipid A. The lipid A fractions were then analyzed by means of MALDI-TOF MS and MS/MS while the carbohydrate portions were further purified by size-exclusion chromatography (SEC) enabling for DSM 2008 to isolate fractions differing for the length of the O-antigen. The NMR investigation of these fractions allowed the identification of the sugar moiety connecting the moiety-antigen to the core OS region and thus to establish the biological repeating unit of DSM 2008 S-LPS. Finally, to a complete structural information on the core OS, NMR analysis of fully deacylated R- and S-LPS after alkaline treatment was also performed.

The ^{1}H and HSQC NMR spectra of the core OS fraction from 118(3) R-LPS (Figures S2 and S3) revealed the presence of six anomeric signals, diagnostic for six spin systems (**A**–**E**, Figure S3; Table S2), which were fully assigned (see Supporting Information for complete chemical and spectroscopic analyses and full structural discussion; Supporting Note 2; Figures S2–S5; Table S2). In addition, H-3 methylene resonances of a Kdo unit (**K**) were also identified in the spectra at δ_H 1.84/1.97 ppm and δ_C 34.0 ppm (Figure S3; Table S2). The assignment of all spin systems was executed by tracing the spin connectivity visible in the DQF-COSY and TOCSY spectra; in parallel, the assignment of each carbon atom was achieved by analyzing the HSQC spectrum.[17] The anomeric configuration of each monosaccharide unit was established by studying the intraresidue NOE correlations observable in the NOESY spectrum and the $^{3}J_{H1,H2}$ coupling constant values attained from the DQF-COSY spectrum, whereas the vicinal $^{3}J_{H,H}$ coupling constants allowed the determination of the relative configuration of each monosaccharide residue.[17] Through this approach, the core OS obtained upon acid treatment of the 118(3) R-LPS was defined as a hexasaccharide made up of one α-Kdo (**K**), two α-L,D-Hep (**A**/**A'** and **B**), two β-D-Glc (**D** and **E**), and one β-D-Gal (**C**). Moreover, the α-L,D-Hep residue **A** was found to carry a 2-aminoethyl phosphate (*P*EtN) unit at its O-6 position, as indicated by the correlation of H-6 **A** with a signal at −0.73 ppm in the ^{31}P,^{1}H HSQC spectrum, which in turn also correlated with methylene proton resonances at δ_H

4.09 and 3.20 ppm (Figure S5). Furthermore, the NMR investigation of full deacylated R-LPS was crucial to identify an additional Kdo unit ($\mathbf{J_{dAc}}$) connected at position O-4 of Kdo $\mathbf{K_{dAc}}$, as also supported by linkage analysis. Analogously, DSM 2008 was found to carry two Kdo (Figure S6, Table S2).

The primary sequence of the core OS was inferred by inter-residue NOE correlations in the NOESY spectrum and the long-range correlations in the HMBC spectrum (Figure 1a). Briefly, Kdo unit (**K**) was substituted at O-5 by α-L,D-Hep **B** as proven by the long-range correlation between H-1 of **B** and C-5 of **K** (Figure 1a); α-L,D-Hep **B** was, in turn, substituted at positions O-3 and O-4 by α-L,D-Hep **A** and β-D-Glc **E**, respectively. α-L,D-Hep **A** in turn, carried the terminal β-D-Glc **D** at its O-2 position. Finally, the observation that also spin system **A**′ showed a long-range correlation with O-4 of **B** suggested that **A**′ was an alternative spin system for residue α-L,D-Hep **A** generated by the non-stochiometric presence of the β-D-Gal (**C**) unit. This was further corroborated by the occurrence of a long-range correlation between H-1 of **C** and H-4 of **A**′ (Figure 1a).

NMR investigation of the highest molecular-weight SEC fraction, obtained after mild acid hydrolysis of the DSM 2008 S-LPS, allowed to define the repeating unit composing the O-antigen moiety (Supporting Note 3; Figures 1b and S7–S9; Table S3). This consisted of a linear zwitterionic trisaccharide sequence containing β-D-Gal*f* (**F**), α-D-Glc*p*N (**G**), β-D-Gal*p* (**H**) and the acyclic hexose alcohol mannitol (**I**) polymerized through a phosphodiester linkage between position O-6 of mannitol **I** and position O-3 of α-D-Glc*p*N (**G**), as confirmed by $^{1}H,^{31}P$ HSQC data (Figure S9).

Finally, the NMR analysis of an intermediate molecular weight SEC fraction allowed (i) to confirm that DSM 2008 and 118(3) strains produce the same core OS structure and (ii) to identify the sugar bridging the O-antigen to the core OS, thus enabling the definition of the complete structure of the DSM 2008 S-LPS. Briefly, it was possible to identify a second, slightly different glycoform of β-D-Glc*p* **D** (Supporting Note 3; Figures 1c and S10, Table S4), referred to here as $\mathbf{D_2}$, which was glycosylated at position O-3. This unit was identified as the sugar carrying the O-antigen moiety, as proven by the long-range correlation between H-1 of $\mathbf{H_2}$ (belonging to the O-antigen) and C-3 of core OS residue $\mathbf{D_2}$ (Figure 1c, Table S4). Therefore, by combining all data attained from above NMR studies, it was possible to establish the complete structure of the carbohydrate portion of both types of LPS, as sketched in Scheme 1 and Figure 2.

Detailed MALDI-TOF MS and MS/MS analyses were conducted on lipid A fractions isolated through mild acid hydrolysis of R- and S-LPS to define their structure (Supporting Note 4). MALDI-TOF MS (Figure 1d) investigation showed that lipid A from the strain 118(3) was a highly complex mixture of species differing in the acylation and phosphorylation profile. Mono- and bisphosphorylated tetra- to hexa-acylated lipid A species were detected, with the latter form presenting a 4+2 distribution of the fatty acid chains with respect to the GlcN disaccharide backbone. An astounding heterogeneity in each lipid A cluster (tetra- to hexa-) was immediately apparent due to the presence of mass differences of 14 atomic mass units (amu; $-(CH_2)-$ unit), indicative of species differing in the length of their acyl chain moieties. By contrast, MALDI-TOF MS spectrum of lipid A from DSM 2008 clearly showed the predominant presence of mono- and bisphosphorylated hexa-acylated lipid A forms. MALDI-TOF mass investigation was also executed directly on bacterial pellets (Figure S11) which confirmed the structures deduced by analysis of the isolated lipid A fractions (Figure 1d). This step was crucial to confirm the structural elucidation and to exclude any lack and/or alteration of structural information possibly occurring as a consequence of the chemical treatment (acid hydrolysis) performed to isolate the lipid A.

The negative-ion MS/MS investigation (Figures S12–S13) of several ion peaks allowed the structural determination of lipid A species. Briefly, the bisphosphorylated hexa-acylated species visible in both spectra at about *m/z* 1796 were assigned to species carrying two 15:0(3-OH) and two 13:0(3-OH) as primary amide- and ester-bound acyl chains, respectively, whereas 13:0 were the two secondary acyl substituents occurring only on the nonreducing GlcN unit. At about *m/z* 1600, bisphosphorylated penta-acylated lipid A species lacking in the secondary acyl chain present in the acyloxyacyl moiety were identified, whereas the bisphosphorylated tetra-acylated lipid A species detected at about *m/z* 1388 matched with lipid A forms devoid of both

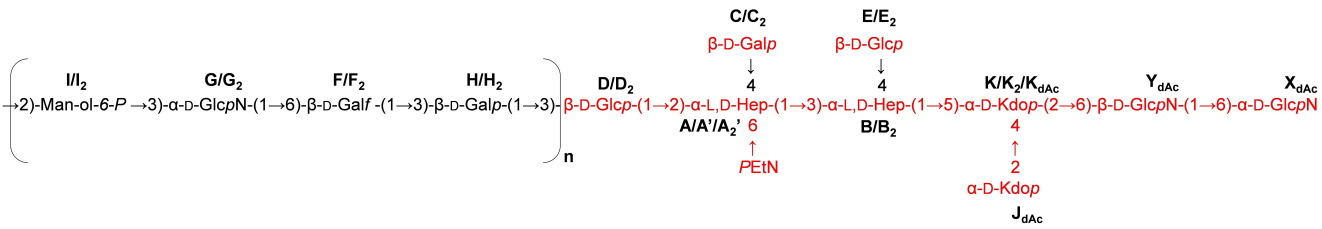

Scheme 1. Structural assessment of the core OS and the O-antigen of *V. parvula*. The carbohydrate structures of R-LPS from *V. parvula* 118(3) and of the S-LPS from *V. parvula* DSM 2008 were determined by merging data from the NMR investigation of the mild acid hydrolysis and full deacylation products. The complete deacylation procedure enabled the isolation of the saccharide fractions plus the lipid A glucosamine disaccharide backbone (labeled as X_{dAc}, Y_{dAc}, Table S2), which also disclosed the occurrence of an additional Kdo unit (J_{dAc}, Table S2). Depicted in red is the structure common between the two strains. Sugar residues are labeled as in Table S2–S4. "*p*" and "*f*" indicate the pyranose and furanose form of sugar units, respectively, whereas "PEtN" indicates the 2-aminoethyl phosphate group.

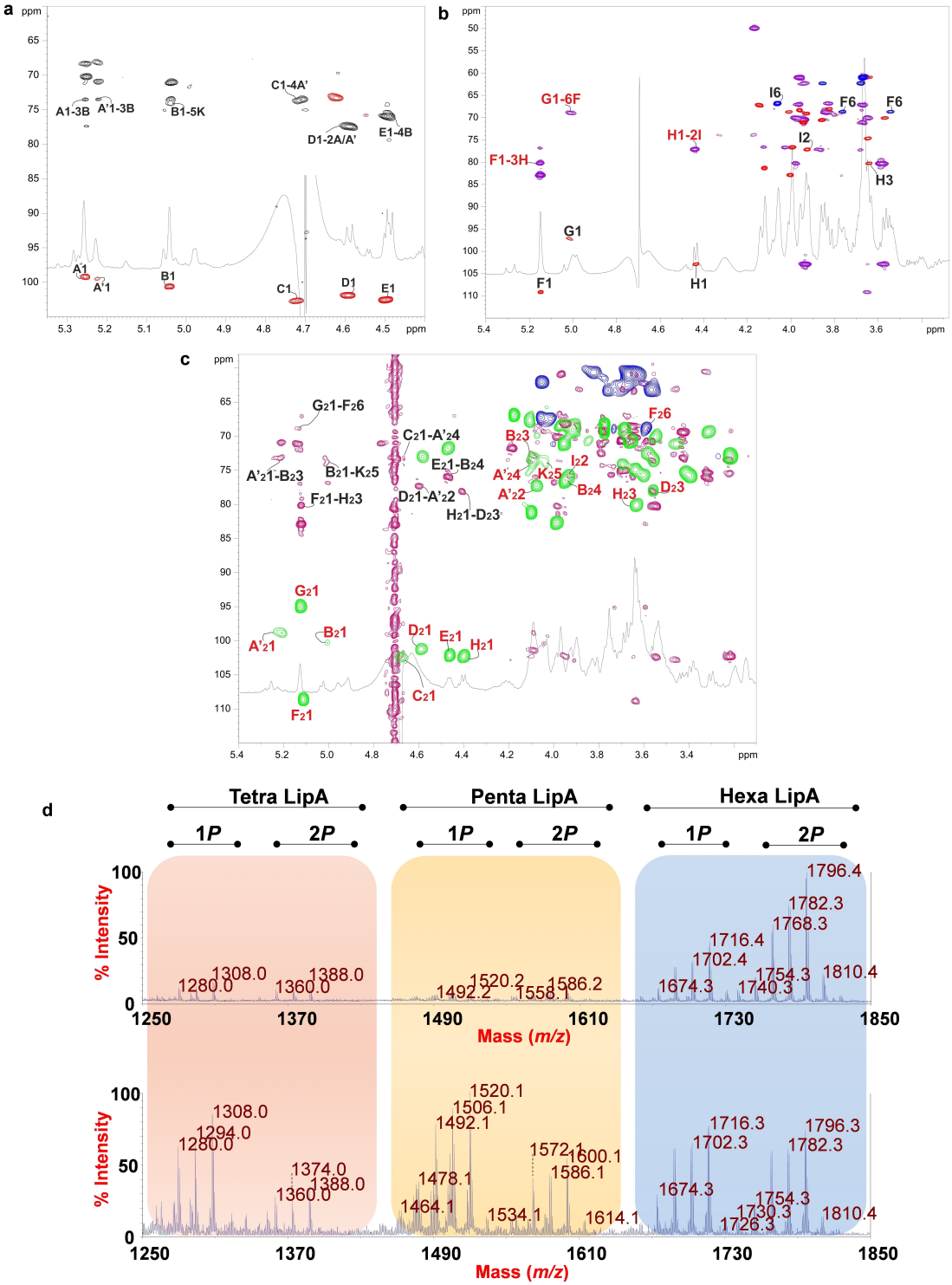

Figure 1. Structural characterization of LPS from *V. parvula*. a) Zoom of the overlapped ^{1}H, ^{1}H, ^{13}C HMBC (black) and ^{1}H, ^{13}C HSQC (red) NMR spectra of the core OS obtained after mild acid hydrolysis of R-LPS from *V. parvula* 118(3). b) Section of the superimposed ^{1}H, ^{1}H, ^{13}C HMBC (purple) and ^{1}H, ^{13}C HSQC (blue and red) NMR spectra of the O-antigen of S-LPS from *V. parvula* DSM 2008. c) Zoom of the overlapped ^{1}H, ^{1}H, ^{13}C HMBC (pink) and ^{1}H, ^{13}C HSQC (green and blue) NMR spectra of the intermediate SEC fraction from mild acid hydrolysis of the S-LPS from *V. parvula* DSM 2008. The key inter-residual long-range correlations involving sugar moieties are reported; letters are as in Tables S2–S4. d) MALDI-TOF MS spectra of the lipid A from *V. parvula* DSM 2008 (up) and *V. parvula* 118(3) (bottom). Colored boxes highlight the clusters of peaks assigned to Tetra-, Penta-, and Hexa-acylated lipid A species, which were labelled as Tetra-, Penta- and Hexa Lip A indicating the degree of acylation. "1*P*" and "2*P*" are indicative of the mono- and bisphosphorylated lipid A species, respectively.

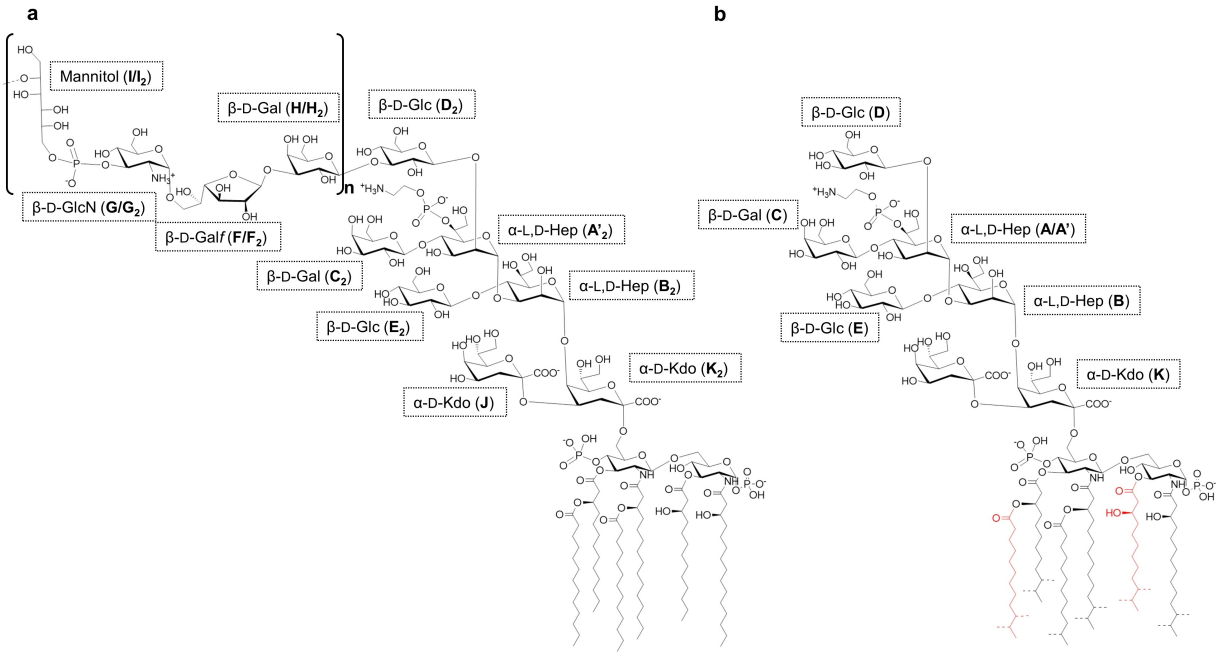

Figure 2. Complete structure of the LPS from *V. parvula*. The full chemical structure of the S-LPS from a) *V. parvula* DSM 2008 and b) R-LPS from *V. parvula* 118(3). The O-antigen repeating unit is indicated in brackets. The letter labels used for NMR analysis are as reported in Tables S2–S4 and Figure 1. Dotted lines indicate that fatty acids can be present in their linear, *iso* and/or *anteiso* branched forms, as reported in Table S1. For *anteiso*-branched acyl moieties the stereochemistry remains to be defined. Red depiction indicates the fatty acids that are missing in the penta- and tetra-acylated lipid A species.

one secondary and one primary *O*-linked fatty acid (Figure S13b). Importantly, all the monophosphorylated lipid A species were shown to carry the phosphate only on the reducing GlcN. An identical structural deduction was obtained for main species visible in the two MALDI-TOF spectra (Figure 1d); nevertheless, based on the chemical composition (Table S1), it is reasonable to hypothesize that lipid A species occurring in the 118(3) strain are characterized by a significant degree of branched-chain fatty acids compared to the lipid A species from the DSM 2008 strain for which no branched acyl chains were detected.

TLR4 activation by V. parvula LPS: Immunological and computational studies

To investigate whether the observed structural differences were reflected into a differential immunological behavior, *V. parvula* S- and R-LPS were tested in the HEK-Blue™ cells transfected with human TLR4, MD-2, and CD14 genes (Figure 3a). Of note, a significant difference between the two LPSs was observed when stimulation was executed by using 1 ng/mL (*V. parvula* R-LPS vs. S-LPS, $p > 0{,}0001$). Indeed, the weaker capability of the R-LPS from the 118(3) to activate the hTLR4 compared to the S-LPS from DSM 2008 was evident. Remarkably, these differences were even more pronounced when the isolated lipid A fractions were tested (*V. parvula* R-LPS vs. S-LPS, $p > 0{,}0001$ at 10 ng/mL; $p > 0{,}001$ at 100 ng/mL, Figure 3a). In addition, to evaluate any potential involvement of other TLRs as previously observed for some gut bacteria[18–20] as well as to exclude the presence of any possible contamination by other immunostimulatory molecules (such as lipoproteins), we also stimulated HEK-Blue™ hTLR2 cells with both types of *V. parvula* LPSs and lipid As. No statistical differences were observed in the NF-kB activation upon stimulation with *V. parvula* S- and R-LPS and their isolated lipid A fractions respect to the negative control (Figure S14). This observation proved that both *V. parvula* LPSs do not activate TLR2-mediated signaling and confirmed the absence of other immunostimulatory molecules co-extracted with the LPSs.

Since it is known that the lipid A is the LPS moiety that directly interacts with TLR4/MD-2 complex, we computationally investigated how the different *V. parvula* lipid A structures interact with this receptor. Docking calculations followed by all-atom molecular dynamics (MD) simulations were performed[21] of a small library of representative *V. parvula* lipid A species towards TLR4 (Supporting Notes 5 and 6; Figures S15–S22). Briefly, for DSM 2008 a bisphosphorylated hexa-acylated lipid A (**$LpA_{DSM2008}$**, Figures 3b and S15) was selected as the representative structure (MALDI TOF *m/z* 1796), and was docked to the agonist conformation of $(TLR4/MD\text{-}2)_2$ system, resulting in binding poses similar to *E. coli* bisphosphorylated hexa-acylated lipid A bound to TLR4 (PDB ID 3FXI), i.e. with the fatty acid chains (FA) inserted into the MD-2 pocket and the disaccharide moiety at the MD-2 rim, and with favorable predicted binding energies. However, the binding was slightly deeper into the MD-2 cavity compared to *E. coli*

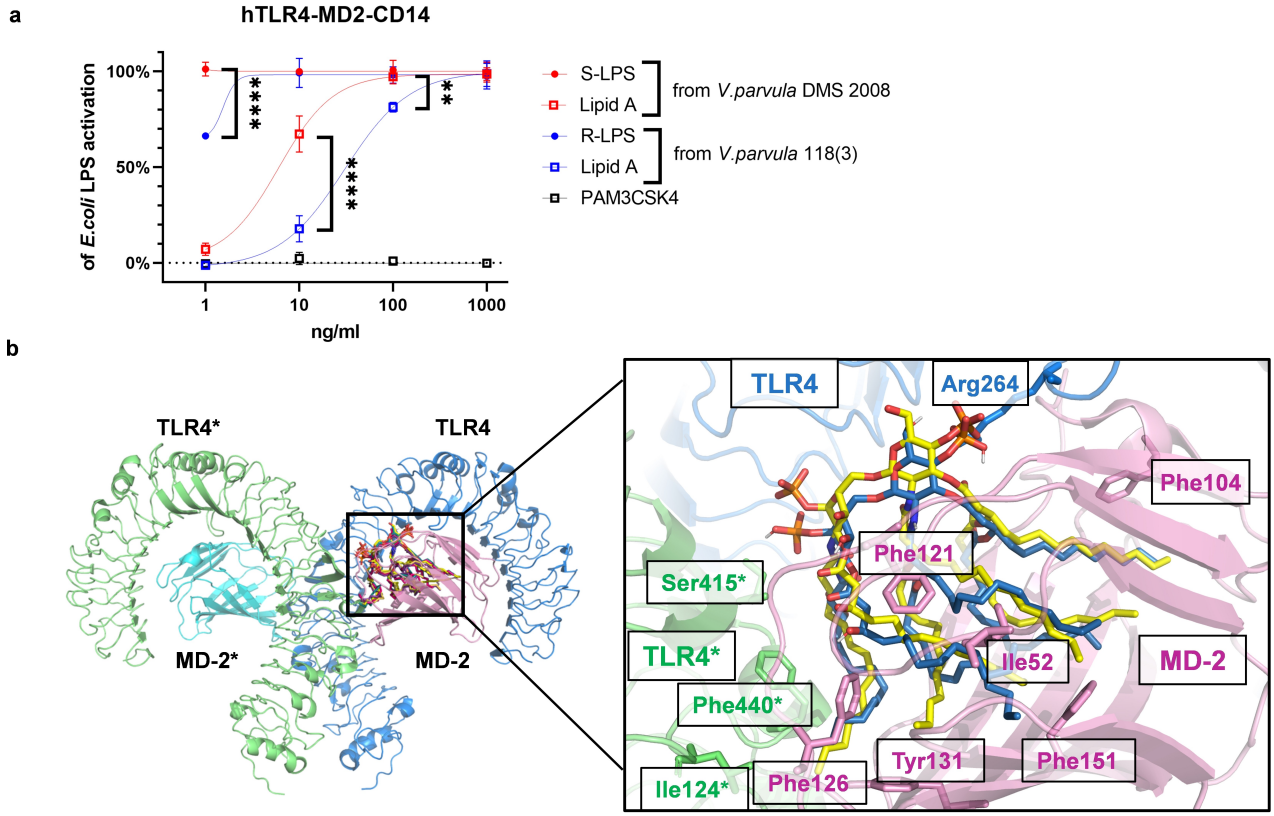

Figure 3. TLR4 activation by *V. parvula* LPS I. a) Stimulation of HEK Blue™ hTLR4. Secreted embryonic alkaline phosphatase (SEAP) levels (OD) upon stimulation with LPS from *E. coli*, *V. parvula* DMS 2008, *V. parvula* 118(3), as well as isolated lipid A from DMS 2008 and 118(3) at the indicated concentrations. PAM3CSK4 was used as the negative control. Data have been normalized on the OD resulted by the stimulation with LPS from *E. coli* and were presented as mean ± S.D. of at least 3 independent experiments which were analyzed using an ordinary two-way ANOVA. Subsequently, multiple comparisons were performed with Sidak's multiple comparison test, with individual variances computed for each comparison, and a statistical significance level of alpha = 0.05. Significance was defined as adjusted *p* value: **** $p < 0.0001$ and ** $p < 0.01$. b) Binding mode of bisphosphorylated hexa-acylated lipid A from *V. parvula* DSM 2008 (**LpA$_{DSM2008}$**, aubergine) to human TLR4/MD-2. The best docked pose calculated from AutoDock Vina and AutoDock4, superimposed with *E. coli* lipid A (PDB ID 3FXI). Left: General view of the extracellular domain of TLR4 with the three best predicted poses for the **LpA$_{DSM2008}$**. TLR4, TLR4*, MD-2 and MD-2* in blue, green, pink and cyan, respectively. Right: Close-up view of the best docked pose of **LpA$_{DSM2008}$** (blue marine) superimposed with *E. coli* lipid A (yellow). Key amino acids involved in the interaction are depicted in sticks.

lipid A (Figure 3b), likely as the result of the shorter FA chains (i.e., primary 13:0(3-OH) and secondary 13:0 in place of 14:0(3-OH) and 14:0, for **LpA$_{DSM2008}$** and *E. coli* lipid A, respectively). As for 118(3), which showed a high degree of structural heterogeneity, several representative lipid A species were investigated: three bisphosphorylated hexa-acylated with different distribution of the *iso* and *anteiso* FA (**BisHexaLpA$_{118(3)}$**) and one monophosphorylated hexa-acylated (**MonoHexaLpA$_{118(3)}$**), one bisphosphorylated (**BisPentaLpA$_{Oral}$**) and its analogous monophosphorylated penta-acylated (**MonoPentaLpA$_{118(3)}$**) species, as well as one bisphosphorylated (**BisTetraLpA$_{118(3)}$**) and the corresponding monophosphorylated tetra-acylated (**MonoTetraLpA$_{118(3)}$**) species (Figure S15). Results suggested that both **LpA$_{intestine}$** and **BisHexaLpA$_{118(3)}$** bind to TLR4/MD-2 in a similar mode to *E. coli* lipid A (PDB ID 3FXI) (Figure 3b and Figure S17a) and engage in interactions with the same residues from the inner cavity of MD-2, despite of the presence of *iso* and *anteiso* branched acyl chains. **BisPentaLpA$_{118(3)}$** species, although less acylated (see inset in Figure S16a), distributed the four acyl chains within the MD-2 pocket with the amide-linked 15:0(3-OH) on the reducing GlcN protruding outside the pocket, maintaining key interactions between the R2' FA chain and the Phe126 loop in MD-2, [22] and residues on the surface of the partner TLR4* (i.e., Phe440, Leu444, and Phe463), thus still mimicking the agonist pose of *E.coli* lipid A (Figure S16a). As for monophosphorylated hexa- and penta-acylated lipid A forms, clear differences were observed in the protein-ligand interactions, with respect to their bisphosphorylated analogues. On one hand, the GlcN backbone of the **MonoHexaLpA$_{118(3)}$** was slightly rotated backwards, reducing the interactions of the GlcN moieties and the ester and amide groups of the lipid chains with MD-2 rim residues (i.e., interactions only with Ser118, Ser120, and Lys122) in comparison to *E. coli* lipid A and the **BisHexaLpA$_{118(3)}$** species. Additionally, the interaction between the 1-phosphate group and Ser415 from the partner TLR4*, key for the completion of the receptor dimerization interface,[22] was lost. Conversely, the 1-phosphate of **MonoPentaL-**

pA$_{118(3)}$ established a H-bond with the Ser415 side chain from TLR4*, as in the case of the bisphosphorylated hexa- and penta-acylated species. Nevertheless, the interaction between the 6'-hydroxyl group of the ligand and the TLR4 Arg264 forced to place the ester-linked primary acyl chain on the nonreducing GlcN oriented backwards, slightly outside the MD-2 cavity, pointing to an unfavorable agonist binding ability (yellow pose in Figure S16b). Of note, our investigation of the bisphosphorylated tetra-acylated species (**BisTetraLpA$_{118(3)}$**) revealed that the 3+1 acylation pattern symmetry, together withthe presence of two phosphate groups on the GlcN backbone, caused the lipid A to be unable to successfully bind inside the MD-2 pocket, regardless of its conformation (Figure S17b). Finally, the docking calculations of *mono*-phosphorylated tetra-acylated lipid A species (**MonoTetraLpA$_{118(3)}$**) to both agonist and antagonist conformations of TLR4, point to a preferential binding into the antagonistic conformation, as none of the poses from the docking in the TLR4 agonist conformation was compatible with the presence of the core OS (Figure S16c).

The stability of the *V. parvula* lipid As in complex with TLR4 was further studied by molecular dynamics (MD) simulations (Supporting Note 6, Figures S18–S22). The agonist conformation of $(TLR4/MD\text{-}2)_2$ was simulated in complex with seven different lipid As. Additionally, the antagonist conformation of the TLR4/MD-2 receptor was simulated in complex with one *mono*-phosphorylated tetra-acylated pose with all FA chains inserted into the MD-2 pocket. Stability was reached by the complexes after 100 ns of simulation (Figures S18–20). Briefly, we observed stable ligand-receptor interactions along the MD simulations for the bisphosphorylated hexa-acylated lipid A of both strains (**LpA$_{DSM2008}$** and **BisHexaLpA$_{118(3)}$**). Moreover, during simulations, both ligands engaged in interactions with the same residues from the inner cavity of MD-2, thus suggesting that the presence of branched acyl chains has no direct effect on the binding of the hexa-acylated ligands into MD-2 (Figures S18–21). On the other hand, simulations of the **BisPentaLpA$_{118(3)}$**, **MonoHexaLpA$_{118(3)}$** and **MonoPentaLpA$_{118(3)}$** highlighted the loss of key protein-ligand interactions, especially with the partner TLR4*,[22] thus pointing to a less efficient capacity in interacting with the receptor in an agonist manner than in the case of the bisphosphorylated hexa-acylated counterparts (Figures S18–20). Finally, for the simulation of the **MonoTetraLpA$_{118(3)}$** in complex with the antagonist conformation of the TLR4, the ligand remained in the pose predicted by docking calculations, resulting in stable ligand-receptor interactions over time (Figure S20), and retaining the antagonist conformation of the MD-2 Phe126 (Figure S19).[23] Remarkably, the distance between the C-terminal and N-terminal domains of TLR4 suffered fluctuations, promoting conformational changes in the horseshoe shaped structure of TLR4, previously reported to interfere in the TLR4 complexation (Figures S18 and S22),[24] pointing to the antagonist modulation capacity of **MonoTetraLpA$_{118(3)}$** towards TLR4. In addition, preliminary docking calculations with the core OS predicted two possible binding poses anchoring TLR4 and also TLR4* (data not shown), and compatible with the lipid As binding poses.

In conclusion, although only a small library of lipid A compounds has been analyzed, overall computational studies suggested that the combination of tetra-acylated lipid A species with the mixture of the other hypo-phosphorylated and hypo-acylated lipid A forms found within the 118(3) R-LPS might explain the weaker activation of the hTLR4 compared to the DSM 2008 S-LPS/lipid A, which is instead predominantly composed of mono- and bisphosphorylated hexa-acylated lipid A species (Figures 1d and 2).

V. parvula LPS activation pathway

To take a glance at the possible distinct molecular activation pathways triggered by *V. parvula* S- and R-LPS, we employed a murine splenic GM-CSF dependent dendritic cell (DC) line, the D1 cells. We performed RT-qPCR on four selected genes known to be involved in the three major LPS-induced pathways: the *tnf-alpha* and *il-1beta* genes as representative of the NF-κB pathway; the *il-2* gene, as representative of the CD14-NFAT pathway, and the Viperin gene, as a representative member of interferon-stimulated genes (ISGs). Early after the addition of stimuli to the cell culture (1 hour), when the NF-κB pathway induces the transcription of inflammatory targets, we observed a significantly weaker activation of DCs when cells were stimulated with 118(3) R-LPS compared to DSM 2008 S-LPS or *E. coli* S-LPS, as evidenced by the transcription of *tnf-alpha* and *il-1beta* genes (Figure 4a). Similar trends were observed when we analyzed the other two pathways 3 hours after stimulation although the results did not reach statistical significance (Figure 4a). Since *il-2* gene is known to be variably regulated, we evaluated protein production as a more stable readout (Figure 4b). A dose response production of the selected cytokines was performed after overnight stimulation. We observed a statistically lower production of both TNFα and IL-2 in response to the 118(3) R-LPS compared to the DSM 2008 S-LPS (Figure 4b). Subsequently, we investigated whether these differences could be partially attributed to the chemical disparities in the lipid A portions. Of note, the results showed that lipid A of 118(3) was significantly less efficient compared to the lipid A of DSM 2008 in eliciting the production of IL-1β and failed in inducing any production of IL-2 and TNFα (Figure 4c,d). Overall, these results proved that the R-LPS from 118(3) has a decreased efficiency in the activation of the three selected pathways downstream of the murine CD14/TLR4/MD-2 complex compared to both DSM 2008 S-LPS and *E. coli* S-LPS.

Differential effect(s) of V. parvula LPSs on human dendritic cells

We then investigated whether human DCs, the sentinel cells of the immune system, respond differently to the S-LPS and the R-LPS. To this purpose, we first used type 2 conventional DCs (cDC2 s), identified as $CD19^{-}BDCA1^{+}$ cells and

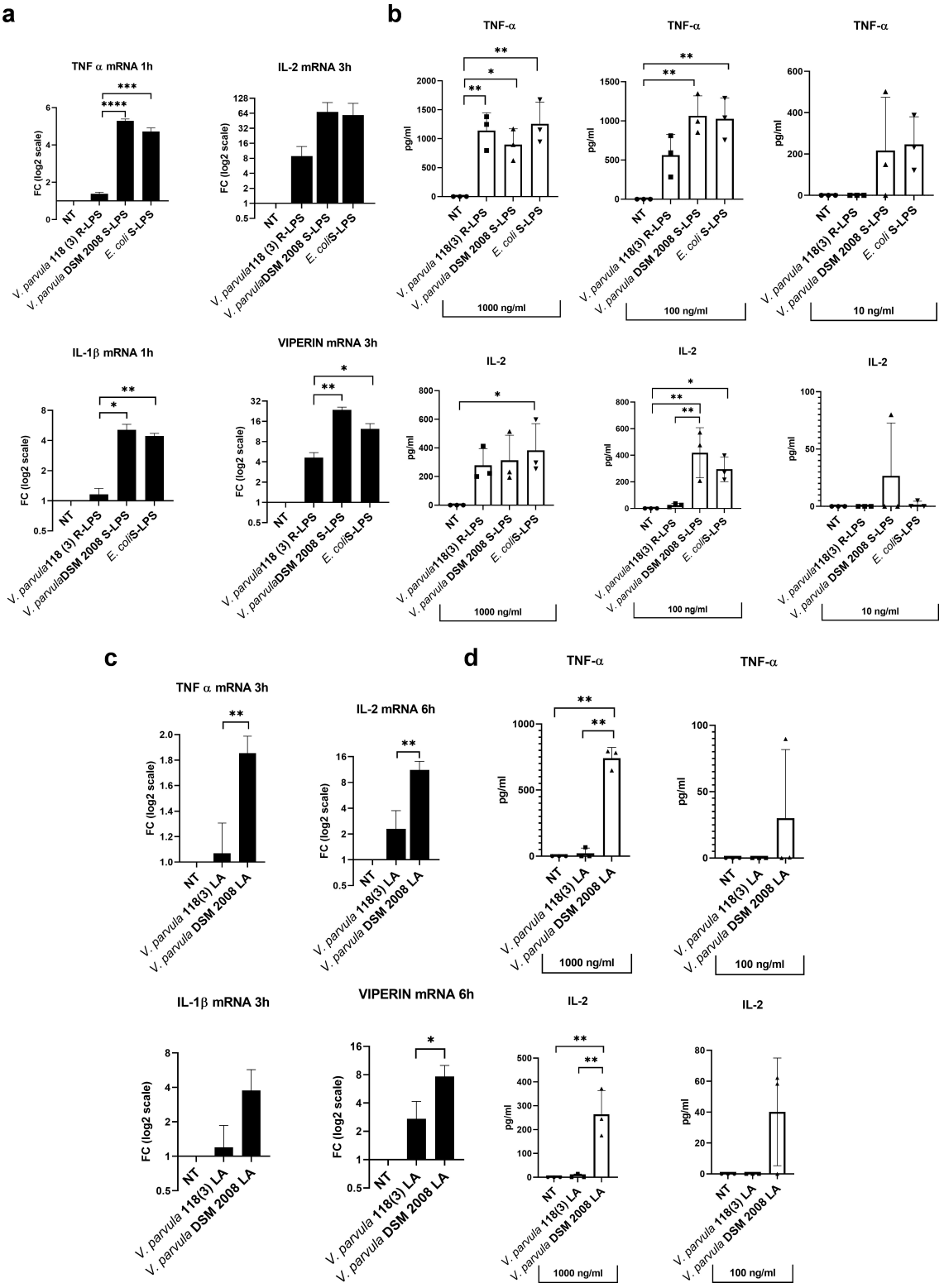

Figure 4. Activation pathways in mouse splenic GM-CSF dependent dendritic cell line by *V. parvula* LPS. a) RT-qPCR analysis of gene expression levels of selected targets (TNF-α, IL-1β, IL-2, and Viperin) normalized on GAPDH following stimulation with LPS from *E. coli*, *V. parvula* DSM 2008, and *V. parvula* 118(3). b) ELISA measurements of cytokine production (TNF-α and IL-2) in response to stimulation with LPS from *E. coli*, *V. parvula* DSM 2008, and *V. parvula* 118(3). c) RT-qPCR analysis of gene expression levels of selected targets (TNF-α, IL-1β, IL-2, and Viperin) normalized on GAPDH following stimulation with lipid A from *V. parvula* DSM 2008 and *V. parvula* 118(3). d) ELISA measurements of cytokine production (TNFα and IL-2) in response to stimulation with lipid A from *V. parvula* DSM 2008 and *V. parvula* 118(3). The time points for RT-qPCR have been adjusted to align with the primary transcriptional accumulation point.

purified from buffy coats of healthy donors. cDC2 s were stimulated overnight with 1000 ng/mL of R- and S-LPS and, initially, a semi-quantitative multi-cytokine array was used to analyze culture supernatants. This assay revealed a slight differential expression of IL-8 when comparing DSM 2008 S-LPS and 118(3) R-LPS. A quantitative ELISA assay showed, then, a significantly higher production of IL-8 by DSM 2008 compared with 118(3) (Figure S23).

In parallel, *V. parvula* S-LPS and R-LPS were also used to stimulate monocyte-derived DCs (MoDCs) isolated from healthy peripheral blood-monocyte-derived DCs. The production of TNF-α, IL-10, and IL-6 was the read-out of these experiments. In general, a weaker pro-inflammatory profile was noticed for both *V. parvula* LPSs compared to *E. coli* (Figures 5a and S24). However, by analyzing different concentrations of the R- and S-LPS (1 and 10 ng/mL), it was possible to observe a significantly lower production of TNF-α upon stimulation with the DSM 2008 S-LPS compared to the 118(3) R-LPS (at 10 ng/mL) (Figures 5a and S24). The observation of such a stronger pro-inflammatory profile of the R-LPS compared to the S-LPS, which contrasted with its weaker TLR4 agonistic activity, led us to hypothesize a "modulating" action exerted by the peculiar structure of the O-antigen portion. Indeed, the crosstalk between different immune pathways induced simultaneously by TLR4 and C-type lectins on MoDCs has been described as a key step for tailoring adaptive and innate responses.[25]

In order to give a first glimpse at such a fascinating and still understudied phenomenon, an exploratory solid-phase assay was performed for the two types of LPSs that were examined for binding to four human C-type lectins (i.e., DC-SIGN, Langerin, Mannose receptor, and MGL) by using Fc-fused C-type lectins constructs (Figure 5b). Strikingly, the DSM 2008 S-LPS showed a stronger binding to DC-SIGN, Langerin and Mannose receptor compared to the 118(3) R-LPS (Figure 5b), thus providing a first indication of a selective and differential recognition of the R- and S-LPS by specific lectins and possibly explaining their divergent pro-inflammatory profiles in MoDCs.

Conclusions

In this study we focused on the LPS isolated from two *V. parvula* strains, the commercial DSM 2008[26] and the clinical isolate 118(3). We observed that the two strains produce LPSs of diverse supramolecular nature (i.e., S-LPS vs. R-LPS), a difference further bolstered by unexpected chemical disparities in the lipid A portion. In fact, the lipid A of DSM 2008 resulted in a mixture of essentially mono- and bisphosphorylated hexa-acylated lipid A species carrying

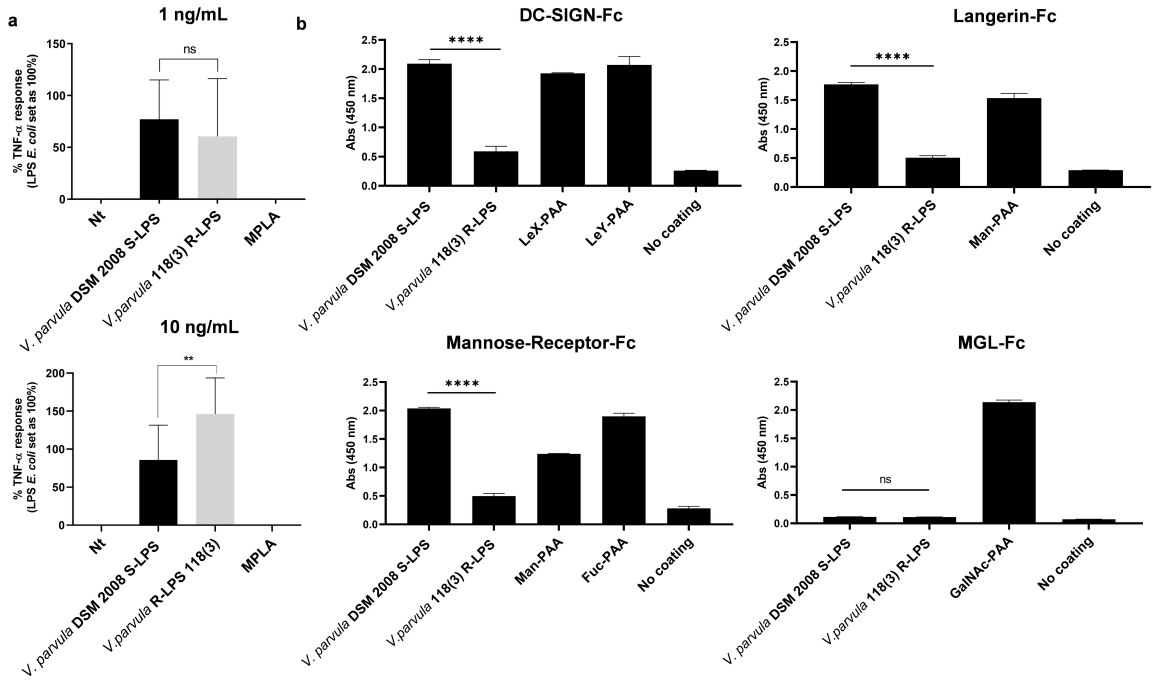

Figure 5. Analysis of immunological properties of *V. parvula* LPS on peripheral blood-monocyte-derived dendritic cells. a) TNF-α release in peripheral blood-monocyte-derived dendritic cells (MoDCs) stimulated with 1 ng/mL (top) and 10 ng/mL (bottom) of *V. parvula* DSM 2008 S-LPS and *V. parvula* 118(3) R-LPS and measured in the supernatants by ELISA. TNF-α data are expressed as percentage of effect/maturation and they are normalized over the MoDCs treated with LPS from *E. coli* (1 and 10 ng/mL, respectively) set at 100% ($n=6$). One-way ANOVA analysis (Tukey's multiple comparisons test with Alpha = 0.05) showed a significant difference (**$p \leq 0.01$) between the S-LPS and the R-LPS. Untreated cells (Nt) and MPLA were used as controls. b) C-type lectins S-LPS and R-LPS binding by solid-phase assay. Plates were coated with the S-LPS and R-LPS and the different C-type lectins Fc-chimera were used to evaluate the binding by ELISA at 450 nm. Polyacrylamide polymers coated with *bona fide* lectins ligands were used as positive controls. One-way ANOVA with Alpha 0.05, the Tukey's multiple comparison test showed a **** $p < 0.001$ value between the *V. parvula* DSM 2008 S-LPS and *V. parvula* 118(3) R-LPS.

unbranched acyl chains. By contrast, the R-LPS-expressing 118(3) strain synthesized a highly complex blend of tetra- to hexa-acylated lipid A species carrying one or two phosphates on the disaccharide backbone, in turn acylated by both branched and unbranched acyl moieties. As 118(3) is a clinical isolate from a pharyngeal swab, this observation tentatively suggests that lipid A branched acyl chains might be key constituents for bacterial adaptation to the oral environment, likely controlling cell membrane fluidity, integrity, and functionality, as previously observed for other bacterial branched-chain fatty acids.[27]

As for the saccharide moieties, the core OS was identical for both strains and was made up of a heptose-containing heptasaccharide whose outermost β-Glc*p* was found to be a terminal residue in the core OS of 118(3), while was further substituted at its O-3 position by a β-Gal*p* in DSM 2008, which thus was identified as the sugar that starts the biological repeating unit of the O-antigen. The latter was found to be built up of an unprecedented mannitol-containing tetrameric repeating unit made up of β-Gal*f*, β-Gal*p*, and α-Glc*p*N, polymerized through a phosphodiester bridge between position O-6 of the mannitol and position O-3 of the α-Glc*p*N. Of note, Vinogradov et al.[28] have recently identified a mannitol phosphate containing O-antigen from another gut bacterium *Fusobacterium nucleatum* strain CTX47T. However, *V. parvula* O-antigen, which is kept together by a phosphodiester bridge between mannitol and the α-Glc*p*N, remains unprecedented not only for the presence of the galactofuranose but also for its zwitterionic nature due to the co-presence of a phosphate and a free amino group within the repeating unit. In addition, to the best of our knowledge, this is the first report about the full structural determination of LPS from a species within the *Veillonella* genus, since so far only rather scant information are available about *Veillonella* LPS structure.[29]

Whether there were scant structural details about *Veillonella* LPS, by contrast, seminal studies have reported on the immunological properties of the LPS from the commercial strain DSM 2008. These studies evidenced its TLR4-dependent capability to induce pro-inflammatory cytokines production in both murine and human in vitro models, although at a less extent compared to *E. coli* LPS, and therefore in accordance to our results.[10,30] Here we have introduced novel and additional molecular and immunomodulatory information by analyzing in parallel the R-LPS from *V. parvula* 118(3). Interestingly, the latter displayed a more pro-inflammatory potential in MoDCs while still behaving as a weaker TLR4 agonist than the S-LPS from DSM 2008. We have attempted to provide a molecular explanation of this behavior by means of computational studies that suggested a role for the astounding chemical heterogeneity of the 118(3) lipid A. In fact, the occurrence of both mono- and bisphosphorylated hexa- and hypo-acylated lipid A forms resulted in the coexistence of putative fully agonist, less efficient agonist, as well as antagonist binding modes that might be responsible for a comprehensive loss of the TLR4 agonist efficiency of the R-LPS. In addition, we also have demonstrated the capability of the lipid A from the DSM 2008 strain to bind agonistically to the receptor but to be placed slightly deeper into the MD-2 pocket in comparison to *E. coli*, which might justify its weaker TLR4 agonistic activity than *E. coli* LPS/lipid A.

Although these results highlight the relevance of producing a heterogeneous blend of lipid A species differing for the acylation and phosphorylation degree to modulate the TLR4 activation, the observation of the higher pro-inflammatory potential of the R-LPS compared to the S-LPS, suggested a role for the O-antigen in somehow dampening/modulating the TLR4-mediated inflammatory response, at least in MoDCs. In this frame, it has been demonstrated that TLR signalling is finely tuned by signals derived by C-type lectins, which bind carbohydrates expressed on cell surface of microbes to tailor immune responses towards either activation or tolerance.[31–35] Therefore, we have started to explore whether the two types of *V. parvula* LPS were also differently recognized by C-type lectins of the human innate immunity system. The four C-type lectins were chosen among those expressed in the gastrointestinal tract and whose activity span from inflammation to immune tolerance depending on several factors including the nature of the ligand.[36–38] This assay clearly evidenced a stronger binding of DC-SIGN, Langerin and Mannose receptor to the S-LPS compared to the R-LPS, which further supported our hypothesis that the O-antigen might modulate, likely via C-type lectins, the TLR4-driven inflammatory response. In this frame, it would be of extreme importance the future use of antagonists/inhibitors to block/inhibit C-type lectins and/or TLR4 to clearly prove the regulatory action of DSM 2008 O-antigen. Nevertheless, the zwitterionic nature of this O-antigen might also have a direct impact on MoDCs response as previously observed for other zwitterionic polysaccharides produced by gut microbes and exerting potent immunomodulatory properties.[39–41] Shedding light on this intriguing phenomenon by also harnessing synthetic derivatives inspired by DSM 2008 O-Antigen is a logical and in progress follow-up of this study.

It is indisputable that perception of complex molecules, such as *V. parvula* LPS, relies on activation of distinct pathways that are interdependent and that might converge at multiple nodes to shape the immune response. However, further studies are needed to demonstrate how this occurs and how LPS structural variations affect recognition, binding, and intracellular signaling. Advances in knowledge of the intricate interplay between immunity receptors and LPS are even more urgent when these interactions occur at the level of the oral and gut mucosa, where they might tip the delicate balance towards tolerance or inflammation. In this context, by this study we meant to provide insight into the structure-to-function relationship of LPS from a prominent human pathobiont to look for and harness the bacterial (carbohydrate and/or lipid) hallmarks that might play an active role in tailoring the host–microbe crosstalk. Deciphering the "chemical language" of these dialogues would definitely offer great opportunities for the development of novel immune therapeutics for bacterial infection disease intervention.

Supporting Information

The authors have cited additional references within the Supporting Information (Ref. [42–72]).

Acknowledgements

This study was supported by the European Research Council (ERC) under the Horizon Europe program under grant agreement No 101039841 (DEBUGGING LPS) and by the project "CLariFY" funded by the MUR Progetti di Ricerca di Rilevante Interesse Nazionale (PRIN) Bando 2022 — grant 2022SHW3KY to F.D.L. and F.C. This work was also supported in part by the Italian Ministry of Foreign Affairs and International Cooperation (Italy-Germany Science and Technology cooperation–Call for joint research proposals for the years 2023–2025). It also benefited of the projects "GiVIng" funded by Prin PNRR 2022 to F.C. and F.D.L. (grant P202293ZMC), and H2020-MSCA-ITN-2020 grant agreement 956758 (GLYTUNES) to A.S., F.B., Y.v.K., and F.C., and by the Spanish Ministry for Science and Innovation (grant PID2020-113588RB-I00) to S.M.S. and (grant PRE2018-086249) to A.M.R.

Conflict of Interest

The authors declare no conflict of interest.

Data Availability Statement

The data that support the findings of this study are available in the supplementary material of this article.

Keywords: Lipopolysaccharides · *Veillonella* · Gut microbiota · Structure–activity relationships · Immunochemistry

[1] P. Zhou, D. Manoil, Belibasakis, G. N. Kotsakis, G. A. Front, *Oral Health* **2021**, *2*, 774115.
[2] D. I. Poppleton, M. Duchateau, V. Hourdel, M. Matondo, J. Flechsler, A. Klingl, C. Beloin, S. Gribaldo, *Front. Microbiol.* **2017**, *8*, 1215.
[3] C. V. Hughes, P. E. Kolenbrander, R. N. Andersen, L. V. Moore, *Appl. Environ. Microbiol.* **1988**, *54*, 1957–1963.
[4] C. W. Africa, J. Nel, M. Stemmet, *Int. J. Environ. Res. Public Health.* **2014**, *11*, 6979–7000.
[5] S. Periasamy, P. E. Kolenbrander, *J. Bacteriol.* **2010**, *192*(12), 2965–2972.
[6] I. Mashima, F. Nakazawa, *J. Bacteriol.* **2015**, *197*, 2104–2111.
[7] A. N. Ananthakrishnan, C. Luo, V. Yajnik, H. Khalili, J. J. Garber, B. W. Stevens, T. Cleland, R. J. Xavier, *Cell Host Microbe* **2017**, *21*, 603–610.
[8] M. Schirmer, L. Denson, H. Vlamakis, E. A. Franzosa, S. Thomas, N. M. Gotman, P. Rufo, S. S. Baker, C. Sauer, J. Markowitz, M. Pfefferkorn, M. Oliva-Hemker, J. Rosh, A. Otley, B. Boyle, D. Mack, R. Baldassano, D. Keljo, N. LeLeiko, M. Heyman, A. Griffiths, A. S. Patel, J. Noe, S. Kugathasan, T. Walters, C. Huttenhower, J. Hyams, R. J. Xavier, *Cell Host Microbe.* **2018**, *24*, 600–610.
[9] P. Lee, B. K. K. Fields, T. Liang, M. P. Dubé, S. Politano, *Case Reports Hepatol.* **2021**, *2021*, 9947213.
[10] Z. Zhan, W. Liu, L. Pan, Y. Bao, Z. Yan, L. Hong, *Cell Death Dis.* **2022**, *8*, 251.
[11] D. F. Rojas-Tapias, E. M. Brown, E. R. Temple, M. A. Onyekaba, A. M. T. Mohamed, K. Duncan, M. Schirmer, R. L. Walker, T. Mayassi, K. A. Pierce, J. Ávila-Pacheco, C. B. Clish, H. Vlamakis, R. J. Xavier, *Nat. Microbiol.* **2022**, *7*, 1673–1685.
[12] F. Di Lorenzo, K. A. Duda, R. Lanzetta, A. Silipo, C. De Castro, A. Molinaro, *Chem. Rev.* **2022**, *122*, 15767–15821.
[13] F. Di Lorenzo, C. De Castro, A. Silipo, A. Molinaro, *FEMS Microbiol. Rev.* **2019**, *43*, 257–272.
[14] C. Galanos, O. Luderitz, O. Westphal, *Eur. J. Biochem.* **1969**, *9*, 245–249.
[15] O. Westphal, O. Lüderitz, F. Bister, . *Naturforsch., B: J. Chem. Sci.* **1952**, *7*, 148–155.
[16] M. D. Pither, A. Silipo, A. Molinaro, F. Di Lorenzo, *Methods Mol. Biol.* **2023**, *2613*, 153–179.
[17] I. Speciale, A. Notaro, P. Garcia-Vello, F. Di Lorenzo, S. Armiento, A. Molinaro, R. Marchetti, A. Silipo, C. De Castro, *Carbohydr. Polym.* **2022**, *277*, 118885.
[18] T. Vatanen, A. D. Kostic, E. d'Hennezel, H. Siljander, E. A. Franzosa, M. Yassour, R. Kolde, H. Vlamakis, T. D. Arthur, A. M. Hämäläinen, A. Peet, V. Tillmann, R. Uibo, S. Mokurov, N. Dorshakova, J. Ilonen, S. M. Virtanen, S. J. Szabo, J. A. Porter, H. Lähdesmäki, C. Huttenhower, D. Gevers, T. W. Cullen, M. Knip; *DIABIMMUNE Study Group*; R. J. Xavier, *Cell* **2016**, *165*, 842–853.
[19] F. Di Lorenzo, M. D. Pither, M. Martufi, I. Scarinci, J. Guzmán-Caldentey, E. Łakomiec, W. Jachymek, S. C. M. Bruijns, S. M. Santamaría, J. S. Frick, Y. Van Kooyk, F. Chiodo, A. Silipo, M. L. Bernardini, A. Molinaro *ACS Cent. Sci.* **2020**, *6*, 1602–1616.
[20] M. D. Pither, A. Illiano, C. Pagliuca, A. Jacobson, G. Mantova, A. Stornaiuolo, R. Colicchio, M. Vitiello, G. Pinto, A. Silipo, M. A. Fischbach, P. Salvatore, A. Amoresano, A. Molinaro, F. Di Lorenzo, *Carbohydr. Polym.* **2022**, *297*, 120040.
[21] A. Matamoros-Recio, J. Merino, A. Gallego-Jiménez, R. Conde-Alvarez, M. Fresno, S. Martín-Santamaría, *Carbohydr. Polym.* **2023**, *318*, 121094.
[22] B. S. Park, D. H. Song, H. M. Kim, B. S. Choi, H. Lee, J. O. Lee, *Nature* **2009**, *458*, 1191–1195.
[23] U. Onto, K. Fukase, K. Miyake, Y. Satow, *Science* **2007**, *316*, 1632–1634.
[24] C. de Aguiar, M. G. Costa, H. Verli, *Proteins* **2015**, *83 (2)*, 373–382.
[25] S. I. Gringhuis, J. Den Dunnen, M. Litjens, M. Van der Vlist, T. B. Geijtenbeek, *Nat. Immunol.* **2009**, *10*, 1081–1088.
[26] S. Gronow, S. Welnitz, A. Lapidus, M. Nolan, N. Ivanova, T. Glavina Del Rio, A. Copeland, F. Chen, H. Tice, S. Pitluck, J. F. Cheng, E. Saunders, T. Brettin, C. Han, J. C. Detter, D. Bruce, L. Goodwin, M. Land, L. Hauser, Y. J. Chang, C. D. Jeffries, A. Pati, K. Mavromatis, N. Mikhailova, A. Chen, K. Palaniappan, P. Chain, M. Rohde, M. Göker, J. Bristow, J. A. Eisen, V. Markowitz, P. Hugenholtz, N. C. Kyrpides, H. P. Klenk, S. Lucas, *Stand Genomic Sci.* **2010**, *2*, 57–65.
[27] H. Lu, Z. Wang, B. Cao, F. Cong, X. Wang, W. Wei, *Food Chem.* **2024**, *431*, 137158.
[28] E. Vinogradov, F. St Michael, C. Cairns, A. D. Cox, *Carbohydr. Res.* **2022**, *521*, 108648.
[29] T. Hofstad, T. Kristoffersen, *Acta Pathol. Microbiol. Scand. Sect. B* **1970**, *78*, 760–764.
[30] G. Matera, V. Muto, M. Vinci, E. Zicca, S. Abdollahi-Roodsaz, F. L. van de Veerdonk, B. J. Kullberg, M. C. Liberto, J. W.

van der Meer, A. Focà, M. G. Netea, L. A. Joosten, *Clin. Vaccine Immunol.* **2009**, *16*, 1804–1809.
[31] M. J. Robinson, D. Sancho, E. C. Slack, S. LeibundGut-Landmann, C. Reis Sousa, *Nat. Immunol.* **2006**, *7*, 1258–1265.
[32] T. B. Geijtenbeek, S. J. Van Vliet, E. A. Koppel, M. C. M. Sanchez-Hernandez, C. M. Vandenbroucke-Grauls, B. Appelmelk, Y. Van Kooyk, *Exp. Med.* **2003**, *197*, 7–17.
[33] D. M. Underhill, *Immunol. Rev.* **2007**, *219*, 75–87.
[34] T. B. Geijtenbeek, S. I. Gringhuis, *Nat. Rev. Immunol.* **2009**, *9*, 465–479.
[35] S. J. Van Vliet, J. Den Dunnen, S. I. Gringhuis, T. B. Geijtenbeek, Y. Van Kooyk, *Curr. Opin. Immunol.* **2007**, *19*, 435–440.
[36] I. G. Zizzari, C. Napoletano, F. Battisti, H. Rahimi, S. Caponnetto, L. Pierelli, M. Nuti, A. Rughetti, *J. Immunol. Res.* **2015**, *2015*, 450695.
[37] C. Castenmiller, B. C. Keumatio-Doungtsop, R. van Ree, E. C. de Jong, Y. van Kooyk, *Front. Immunol.* **2021**, *12*, 643240.
[38] Y. van Kooyk, *Biochem. Soc. Trans.* **2008**, *36*, 1478–1481.
[39] S. A. Hsieh, P. M. Allen, *Front. Immunol.* **2020**, *11*, 690.
[40] S. K. Mazmanian, D. L. Kasper, *Nat. Rev. Immunol.* **2006**, *6*, 849–858.
[41] D. Erturk-Hasdemir, J. Ochoa-Repáraz, D. L. Kasper, L. H. Kasper, *Front. Immunol.* **2021**, *12*, 662807.
[42] R. Kittelberger, F. Hilbink, *J. Biochem. Biophys. Methods* **1993**, *26*, 81–86.
[43] P. Garcia-Vello, I. Speciale, F. Di Lorenzo, A. Molinaro, C. De Castro, *Methods Mol. Biol.* **2022**, *2548*, 181–209.
[44] E. T. Rietschel, *Eur. J. Biochem.* **1976**, *64*, 423–428.
[45] E. G. Bligh, W. J. Dyer, *Can. J. Biochem. Physiol.* **1959**, *37*, 911–917.
[46] O. Holst, J. E. Thomas-Oates, H. Brade, *Eur. J. Biochem.* **1994**, *222*, 183–194.
[47] A. S. Stern, K. B. Li, J. C. Hoch, *J. Am. Chem. Soc.* **2002**, *124*, 1982–1993.
[48] F. Di Lorenzo, *Antonie van Leeuwenhoek* **2017**, *110*, 1401–1412.
[49] G. Larrouy-Maumus, A. Clements, A. Filloux, R. R. McCarthy, S. Mostowy, *J. Microbiol. Methods.* **2016**, *120*, 68–71.
[50] U. Manual, *Schrödinger Release* 2018–3: LigPrep, Schrödinger, LLC, New York, NY, **2018**.
[51] E. Harder, W. Damm, J. Maple, C. Wu, M. Reboul, J. Y. Xiang, L. Wang, D. Lupyan, M. K. Dahlgren, J. L. Knight, J. W. Kaus, D. S. Cerutti, G. Krilov, W. L. Jorgensen, R. Abel, R. A. Friesner, *J. Chem. Theory Comput.* **2016**, *12*, 281–296.
[52] PyMOL | pymol.org https://pymol.org/2/ (accessed Jun 15, 2020).
[53] M. J. Frisch, et al. *Gaussian 09*, Revision A.02. Gaussian, Inc., Wallingford CT **2016**.
[54] D. A. Case, R. M. Betz, D. S. Cerutti, T. E. Cheatham III, T. A. Darden, R. E. Duke, T. J. Giese, H. Gohlke, A. W. Goetz, N. Homeyer, *AMBER 2016 Reference Manual.* Univ. Calif. San Fr. CA, USA **2016**, 1–923.
[55] J. Wang, W. Wang, P. A. Kollman, D. A. Case, *J. Mol. Graphics Modell.* **2006**, *25*, 247–260.
[56] C. I. Bayly, P. Cieplak, W. D. Cornell, P. A. Kollman, *J. Phys. Chem.* **1993**, *97*, 10269–10280.
[57] J. Wang, R. M. Wolf, J. W. Caldwell, P. A. Kollman, D. A. Case, *J. Comput. Chem.* **2004**, *25*, 1157–1174.
[58] K. N. Kirschner, A. B. Yongye, S. M. Tschampel, J. González-Outeiriño, C. R. Daniels, B. L. Foley, R. J. Woods, *J. Comput. Chem.* **2008**, *29*, 622–655.
[59] C. J. Dickson, B. D. Madej, Å. A. Skjevik, R. M. Betz, K. Teigen, I. R. Gould, R. C. Walker, *J. Chem. Theory Comput.* **2014**, *10*, 865–879.
[60] O. Trott, A. J. Olson, *J. Comput. Chem.* **2010**, *31*, 455–461.
[61] G. M. Morris, H. Ruth, W. Lindstrom, M. F. Sanner, R. K. Belew, D. S. Goodsell, A. J. Olson, *J. Comput. Chem.* **2009**, *30*, 2785–2791.
[62] J. A. Maier, C. Martinez, K. Kasavajhala, L. Wickstrom, K. E. Hauser, C. Simmerling, *J. Chem. Theory Comput.* **2015**, *11*, 3696–3713.
[63] U. Essmann, L. Perera, M. L. Berkowitz, T. Darden, H. Lee, L. G. Pedersen, *J. Chem. Phys.* **1995**, *103*, 8577–8593.
[64] D. R. Roe, T. E. Cheatham, *J. Chem. Theory Comput.* **2013**, *9*, 3084–3095.
[65] M. J. Abraham, T. Murtola, R. Schulz, S. Páll, J. C. Smith, B. Hess, E. Lindah, *SoftwareX* **2015**, *1–2*, 19–25.
[66] W. Humphrey, A. Dalke, K. Schulten, *J. Mol. Graphics* **1996**, *14*, 33–38.
[67] C. Winzler, P. Rovere, M. Rescigno, F. Granucci, G. Penna, L. Adorini, V. S. Zimmermann, J. Davoust, P. Ricciardi-Castagnoli, *J. Exp. Med.* **1997**, *185*, 317–328.
[68] Q. Zhu, Z. Shen, F. Chiodo, S. Nicolardi, A. Molinaro, A. Silipo, B. Yu, *Nat. Commun.* **2020**, *11*, 4142.
[69] G. I. Birnbaum, *J. Carbohydr. Chem.* **1987**, *6*, 17–39.
[70] Y. Wang, W. M. Kalka-Moll, M. H. Roehrl, D. L. Kasper, *Proc. Natl. Acad. Sci. USA* **2000**, *97*, 13478–13483.
[71] B. Domon, C. E. Costello, *Glycoconjugate J.* **1988**, *5*, 397–409.
[72] D. Chen, N. Oezguen, P. Urvil, C. Ferguson, S. M. Dann, T. C. Savidge, *Sci. Adv.* **2016**, *2*, e1501240.

Manuscript received: January 22, 2024
Accepted manuscript online: February 23, 2024
Version of record online: March 8, 2024